

## Ionization (Shakeoff) Accompanying $K$ -Shell Internal Conversion\*

F. T. Porter, M. S. Freedman, and F. Wagner, Jr.

*Chemistry Division, Argonne National Laboratory, Argonne, Illinois 60439*

(Received 18 December 1970)

Magnetic  $\beta$ -ray spectrometer studies at 0.05% momentum resolution with isotope-separator-prepared samples have revealed structure below the  $K$  conversion lines of the 122- and 136-keV ( $\text{Fe}^{57}$ ) and the 661-keV ( $\text{Ba}^{137}$ ) transitions. This structure consists of an abrupt rise below the  $K$  conversion line (in atomic number  $Z$ ) at an energy displacement approximately equal to the  $L_3$  binding in the  $(Z+1)$  neutral atom, and a continuum extending to lower energies. These continua are interpreted as the spectra complementary to the (unobserved; energy near zero)  $L$ -shakeoff spectra; i.e., the sum of ejected  $K$ - and  $L$ -electron energies equals a constant. The double-vacancy binding energy for  $KL_3$  is  $7905^{+20}_{-10}$  eV for Fe and  $43.01 \pm 0.03$  keV for Ba. The sum of  $KL$  shakeoff from all three  $L$  subshells compared with the  $K$  line is  $\sum KL/K = 9 \times 10^{-3}$  for Fe and  $1 \times 10^{-3}$  for Ba (both with uncertainties estimated at  $\sim 50\%$ ), in good agreement with self-consistent-field overlap integrals for shakeoff in  $\beta^-$  decay if one takes the effective charge change for  $L$  electrons during  $K$  conversion as  $\sim 0.85$  times that for  $\beta^-$  decay. The spectrum shape of the  $KL$  continua, in the main, confirms the predictions of the nonrelativistic calculations which have been made for  $\beta$ -decay processes, but some discrepancies are suggested. For the less probable  $K$  shakeoff accompanying  $K$  conversion, preliminary values for intensities of the continua with respect to the  $K$  line are  $KK/K$  between  $(0.4-2) \times 10^{-4}$  for Fe, and  $KK/K < 2 \times 10^{-4}$  for Ba. No  $M_1$  or  $M_2, 3$  shakeoff was obvious on the  $K$  line of the 14-keV transition in  $\text{Fe}^{57}$ .

### I. INTRODUCTION

We report here the first observation of structure on  $K$  internal-conversion lines which can be interpreted as the result of the sudden change in the Coulomb field accompanying the internal-conversion process. Similar shakeoff processes<sup>1</sup> have been studied theoretically and experimentally for  $\beta^+$  decay,  $\alpha$  decay, orbital-electron-capture decay, photoelectric events, and electron impact interactions.

The observed result of the process being discussed here is depicted schematically in Fig. 1, which shows an electron energy spectrum. Under ideal conditions, a  $K$  internal-conversion line in element  $Z$  might be observed as indicated on the right-hand side of the figure. Normal  $K$  conversion results in one electron in the final state; however, with relatively low probability, the sudden change in the Coulomb field ejects a partner orbital electron which shares the available energy. With two electrons in the final state a continuum results, rather than a monoenergetic line. Because of the nature of the shakeoff process, the most probable partition of the energy is that one electron has a very low energy and the other has nearly the maximum available. In Fig. 1, for example, the dashed curves labeled  $L$  represent the continuum for a  $K$  and  $L$  electron ejected in the final state, and the solid curves labeled  $K$  indicate the continuum for both  $K$  electrons ejected in the final state. The shape of the low-energy part of the

continuum is expected to be similar to that of shakeoff electron spectra calculated for  $\beta$ -decay processes, i.e., some strong inverse function of the energy. It follows from the conservation of energy that the complementary electron partner will have an energy spectrum which is just a mirror image of the shakeoff energy spectrum. Thus, the total continuum can be thought of as the sum of the shakeoff spectrum and the mirror-image complementary electron spectrum, each of these extending from zero energy up to the maximum available energy.

This maximum available energy is just the transition energy minus the energy required to remove from the atom, simultaneously, the two electrons in question (just as the normal  $K$ -conversion-line energy is the transition energy minus the  $K$  binding energy). We have indicated in Fig. 1 that the structure associated with  $L$  shakeoff accompanying  $K$  conversion might be expected at about the  $L$  binding energy for  $Z+1$  below the  $K$  conversion line, and, similarly, the  $K$  shakeoff structure might be expected at about the  $K$  binding energy for  $Z+1$  below the  $K$  line. This expectation is based on the approximation that the  $K$ -electron screens at most one unit of the nuclear charge, so that on its removal from an atom of atomic number  $Z$ , the work necessary to remove an  $L$  electron or the second  $K$  electron would be at most the binding energy in the  $Z+1$  neutral atom. Our results, in fact, show that in the case of  $L$  structure, the additional binding energy be-

low the  $K$  line is slightly *greater* than that of the  $L$  electron in  $Z+1$ .

The schematic Fig. 1 also conveys the expectation that  $K$  shakeoff accompanying  $K$  conversion is less probable than  $L$  shakeoff accompanying  $K$  conversion; it is, in fact, relatively much less than the figure indicates. For example, in Fe ( $Z=26$ ),  $K$  shakeoff/ $L$  shakeoff  $\approx 10^{-2}$  from our experiments. Omitted from Fig. 1 are similar continua derived from the other shells ( $M$ ,  $N$ , etc.) which are presumably there, but, of course, are even closer to the original  $K$  conversion line. For the cases we investigated they are so close to the normal  $K$  conversion line that they are not resolvable with our instrumentation, except for the case of the  $K$  line of the 14-keV transition (see Sec. E).

The direct observation of the very low-energy shakeoff spectrum with any accuracy is very difficult, for the usual experimental reasons involving source problems and scattering. However, because the complementary electron spectrum is just the mirror image of the shakeoff spectrum, it offers a way to study the shape of the shakeoff spectrum. This was pointed out in the work of Krause, Carlson, and Dismukes<sup>2</sup> on the closely

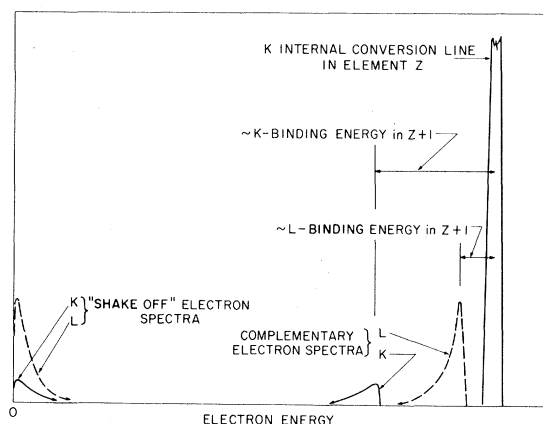


FIG. 1. Schematic view of  $K$ - or  $L$ -electron ejection accompanying  $K$  internal conversion. The ordinate is the counting rate in an electron energy spectrometer. At the right-hand side is shown the lower portion of a  $K$  conversion line for a nuclear transition in element  $Z$ . When two electrons ( $K+K$  or  $K+L$ ) are ejected the resultant continua are displaced to lower energy. These continua are composites of a shakeoff component, whose major contribution occurs at very low energy, and the complementary component (the high-energy partner), whose shape is just the mirror image of the shakeoff components because the sum of the energy of the two electrons is constant, namely, the end-point energy of the continuum. In the present paper we are looking at the high-energy end of these continua (the complementary component), which are displaced below the  $K$  line by an energy approximately equal to the appropriate shell binding energy in an atom of atomic number  $Z+1$ .

related case of shakeoff accompanying  $K$ -shell photoelectron ejection in rare-gas atoms. They have found structure in the electron spectra below the  $K$  photoelectron lines which can be interpreted as  $L$  and  $M$  electrons ejected simultaneously with the  $K$ -shell electrons, a structure quite similar to that being presented here for the case of internal conversion.

Before going into the details of the experimental work, we make three remarks. First, energy considerations make it impossible to distinguish between  $L$  shakeoff with  $K$  conversion, and  $K$  shakeoff with  $L$  conversion, as far as the upper limit of the continuum is concerned. The final state of the atom is the same; namely a hole in both  $K$  and  $L$  shells. Therefore, we shall refer, in what follows, to the curves labeled  $L$  in Fig. 1. as the  $KL$  spectrum or bump, and include both contributions. Actually, in calculations of the two different contributions,  $L$  shakeoff with  $K$  conversion should be the more important channel by orders of magnitude, since the change in the  $L$ -electron environment with departure of a  $K$  electron is far more severe than vice versa. Further, the calculated spectrum shapes are different. We ignore  $K$  shakeoff with  $L$  conversion hereafter.

Second, the decay mode described here should not be confused with the even less probable mode called "double internal conversion,"<sup>3</sup> which occurs by a second-order interaction of the nuclear electromagnetic field with two atomic electrons. While the final atomic state is the same, i.e., two holes in the atomic shells, the energy spectrum of the emitted electrons is quite different. The change in the Coulomb field experienced by the electron cortege, and also, therefore, the shape of the shakeoff spectrum accompanying internal conversion, is independent of the multipolarity of the nuclear transition, and results in emission almost exclusively near "zero" and near the maximum energy of the continuum. On the other hand, the theoretical spectrum shape in the case of double internal conversion depends on the multipolarity of the transition, but, in general, it is not concentrated at the "ends" of the continuum.

Third, in experiments involving ejection of a primary charged particle ( $e^-$ ,  $\beta^+$ ,  $\alpha$ ) sometimes accompanied by an orbital electron, the competition of the direct-collision processes with the shakeoff mechanism must be considered. Direct collision (D.C.) refers to a two-step process in which the first step is the ejection of the charged particle and the second its interaction with an atomic electron of the same atom, both particles emerging in final continuum states. An estimate of the relative probability of D.C. vs shakeoff (Sh) in  $\beta^-$  decay has been given by Feinberg<sup>4</sup>; namely,

D.C./Sh  $\approx$  B.E./ $E$ , where B.E. is the binding energy of the electron to be knocked out and  $E$  is the original kinetic energy of the emitted  $\beta$  particle. In the  $KL$  cases which we consider, this estimate predicts D.C. events  $\sim 10^{-2}$  of shakeoff, even allowing for  $\sim 30\%$  lower probability of  $L$  shakeoff with  $K$  conversion than with  $\beta^-$  decay. In the  $KK$  cases, the D.C. contribution could be significant. (See Sec. II D.) In experiments<sup>5-7</sup> involving  $K$ -x-ray- $\beta^-$  coincidences for pure  $\beta^-$  emitters, no evidence for D.C. contributions has been found in the cases so far investigated. In electron-impact studies<sup>8</sup> on rare gases as a function of incident electron energy, some evidence for small D.C. contributions to double-vacancy final states may exist, but the interpretation is not certain.

The present paper is a high-resolution  $\beta$ -ray spectrometer study of the energy region below several  $K$ -internal-conversion lines, in which it is shown that structure exists at the appropriate energy, and with the appropriate intensity, to be interpreted as the result of the shakeoff process.

## II. EXPERIMENTAL RESULTS

### A. Instrumental

For these experiments, the Argonne toroidal-field iron-free  $\beta$ -ray spectrometers<sup>9</sup> were operated in tandem. The first spectrometer forms an image in the midplane between the machines, and

the second spectrometer, using this image effectively as a source, forms the final image at the detector. With a 1-mm-diam source and a final detector aperture of 1.5 mm, the resolution is 0.05% (full width at half maximum) in momentum and the measured transmission is 4.5% of  $4\pi$ . The angles of emergence of the electrons from the source were between 40 and 70° from the normal to the source plane.

Sources were prepared in the Argonne electromagnetic isotope separator by allowing the ions, decelerated to  $< 25$ -eV energy, to impinge on the source backing through a 1-mm-diam mask. The deceleration of the ions insures negligible penetration into the backing. A thin source is an obvious requirement, since the structure sought lies immediately on the low-energy side of the line where source thickness "tailing" would provide an undesirable background continuum of electrons. From the current in the mass-57 beam of the isotope separator integrated over the time of collection, one calculates on the order of  $\frac{1}{4}$  monolayer for a 5- $\mu$ Ci  $\text{Co}^{57}$  source on a 1-mm-diam deposit. Backscattering from the source backing also results in an undesirable continuum. In this respect, our experiments are less than optimum since we used essentially infinitely thick backings. For reasons which are related to the problem of observing these effects on very low-energy lines, the backings used were surfaces exposed by cleaving nat-

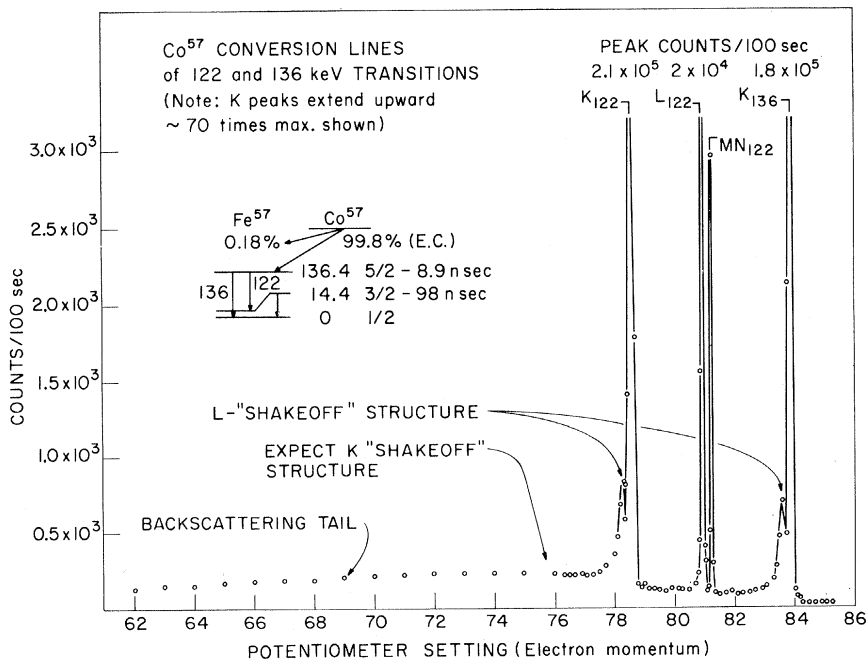


FIG. 2. A vertically magnified view of the base of the indicated conversion lines in the decay  $\text{Co}^{57} \rightarrow \text{Fe}^{57}$ . An abbreviated decay scheme is shown in the inset giving the energies in keV, spins, parities, and half-lives of the states of interest. Arrows indicate where shakeoff structure would be expected. Data are from an  $\sim 80$ - $\mu$ Ci source.

ural graphite crystals mounted with good electrical conductivity to aluminum foils.

### B. $KL$ Continuum

Figure 2 shows the electron momentum spectrum in the neighborhood of the  $K$ ,  $L$ , and  $MN$  internal-conversion lines of the 122-keV transition and the  $K$  line of the 136-keV transition in the decay of  $\text{Co}^{57}$  (conversion taking place in the daughter  $\text{Fe}^{57}$ ). Note that the  $K$  lines extend upward  $\sim 70$  times the maximum ordinate shown. Arrows indicate the position below the  $K$  lines at which we expect to see the  $KL$  and  $KK$  bumps. Indeed, even in this condensed view, the  $KL$  bump is depictable at the base of the  $K$  lines.

Figures 3 and 4 show the  $K_{122}$  and  $K_{136}$  lines in the region of the  $KL$  bump (i.e., the upper end of the  $KL$  continuum), and Fig. 5 shows the  $KL$  bump on the  $K$  line of the 661-keV transition in  $\text{Ba}^{137}$  following the decay of  $\text{Cs}^{137}$ .

The first point to be made is that the bump is not some feature of the focusing of the spectrometer, because the ratio of the momentum of the

bump to the momentum of the main  $K$  peak is not a constant for all cases. Rather, the bump position is related to the  $L$ -binding-energy spacing below the main  $K$  peak. The vertical marks labeled  $L_1$ ,  $L_2$ , and  $L_3$  indicate a momentum position corresponding to the energy of the main  $K$  line reduced by the indicated shell binding energies (shown for  $Z$ ,  $Z+1$ , and  $Z+2$ , where  $Z$  is the atomic number of the element in which the conversion takes place).

Secondly, the intensities are the same order of magnitude as theoretically expected. In order to support this statement, we must define the experimental intensity of the  $KL$  continuum, a task which is not clear-cut, since the tailing off of the complementary continuum, in principle, extends down to zero energy (see Introduction). We need take account only of the complementary continuum, since each shakeoff event results in one electron in the shakeoff continuum and one in the complementary continuum. (The complementary continuum will include a small contribution of electrons associated with the promotion of  $L$  electrons to unoccupied bound states.) However, we can enjoy

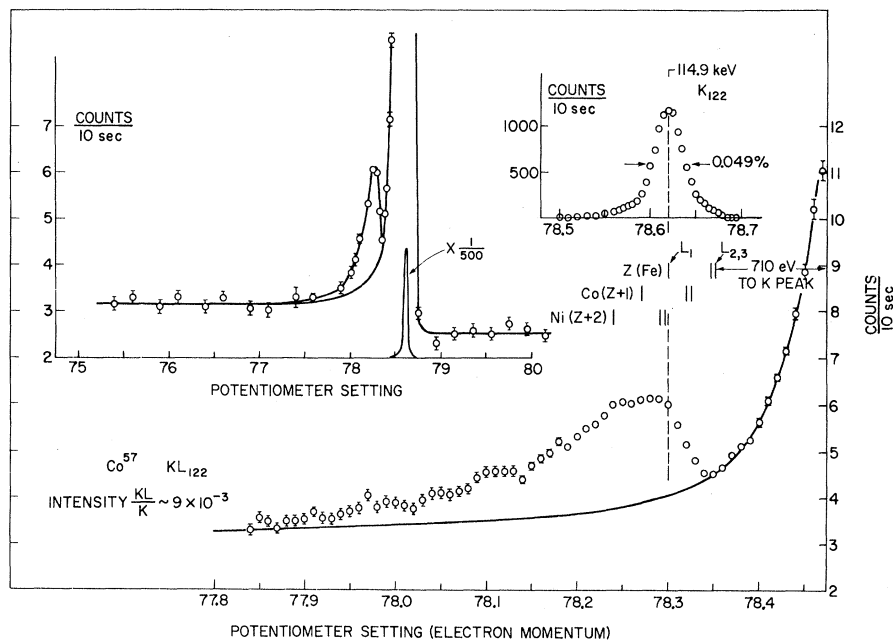


FIG. 3.  $KL$  shakeoff continuum from the 122-keV transition following the decay of  $\text{Co}^{57}$ . Two different momentum expansions are shown in upper-left and lower figures. The inset in the upper right shows the  $K$  line of the 122-keV transition (in the same momentum expansion as the lower figure), illustrating the instrumental-resolution function which must be taken into account in determining where the  $KL_3$  continuum begins. The position of this inset, relative to the lower momentum scale, from a graphical-fitting attempt (see text) to determine this end point. The energy displacements from the peak of the  $K$  line, equal to the  $L$ -shell binding energies in (the daughter) Fe and also in Co and Ni, are indicated. The "tail" of the main  $K$  line, extended under the  $KL$  continuum, is subtracted from the experimental points, yielding an area relative to the  $K$ -line area as indicated in the intensity ratio  $KL/K$ . The asymmetry of the  $K$  line seen in the upper-left plot results from source backing and thickness effects, and possibly from shakeoff from outer shells which would appear displaced from the peak of the  $K$  line by energies less than the linewidth. Data are from a  $\sim 5\text{-}\mu\text{Ci}$  source.

TABLE I. Intensity of  $KL$  shakeoff to  $K$  conversion.

$Z^A$ (transition in keV)	Experimental		Theory	
	$\sum KL/K$	$\sum L/\beta^-$ decay <sup>a</sup>	$\sum KL/K$ <sup>b</sup>	
$^{57}_{26}\text{Fe}$ (122)	$9 \times 10^{-3}$	$1.29 \times 10^{-2}$	$9.5 \times 10^{-3}$	
$^{57}_{26}\text{Fe}$ (136)	$9 \times 10^{-3}$	$1.29 \times 10^{-2}$	$9.5 \times 10^{-3}$	
$^{137}_{56}\text{Ba}$ (661)	$1 \times 10^{-3}$	$1.9 \times 10^{-3}$	$1.4 \times 10^{-3}$	

<sup>a</sup>Reference 10. Sum of  $L_1$ ,  $L_2$ , and  $L_3$  shells.

<sup>b</sup>Previous column multiplied by  $(0.85)^2$  to account for different effective change in charge ( $\beta^-$  decay vs  $K$  conversion) experienced by  $L$  electrons. See Ref. 10.

some after-the-fact assurance in a feature of the shakeoff theory which says that the fraction of the continuum area below 2 or 3 times the binding energy of the ejected shakeoff electron is small ( $<10\%$ ). Proceeding in an obvious way, if the back-scattering tail in Figs. 3-5 is joined smoothly with the main line (by eye), the areas relative to the main  $K$  peaks are obtained. Table I lists the results for the three cases. While it is difficult to assign uncertainties to the experimental values and, indeed, also to the theoretical numbers, conservative judgement indicates 50% on either should include the uncertainties, in which case there is better than order-of-magnitude agreement of the  $KL$  intensity with theoretical expectations.

Thirdly, the bump is not associated with photon interaction with material of the source or spec-

trometer. This is clear from a comparison of the 122- and 136-keV transitions in  $\text{Fe}^{57}$ . Here are two transitions of nearly the same energy in the same source, but their conversion coefficients are different by a factor of 10. There are 10 times as many 122-keV  $\gamma$  rays per electron as there are 136-keV  $\gamma$  rays per electron, yet the  $KL$  bump intensity relative to the main  $K$  line is the same in both cases. Finally, we can point out that the bumps do not have the shape of conversion lines and thus are not the fortuitously situated conversion of some undiscovered transition in these decays, or of some impurity in the mass-separator-prepared samples.

In light of these points, we are persuaded that this structure is not an instrumental effect, and can be interpreted as the  $KL$  shakeoff accompanying  $K$  internal conversion.

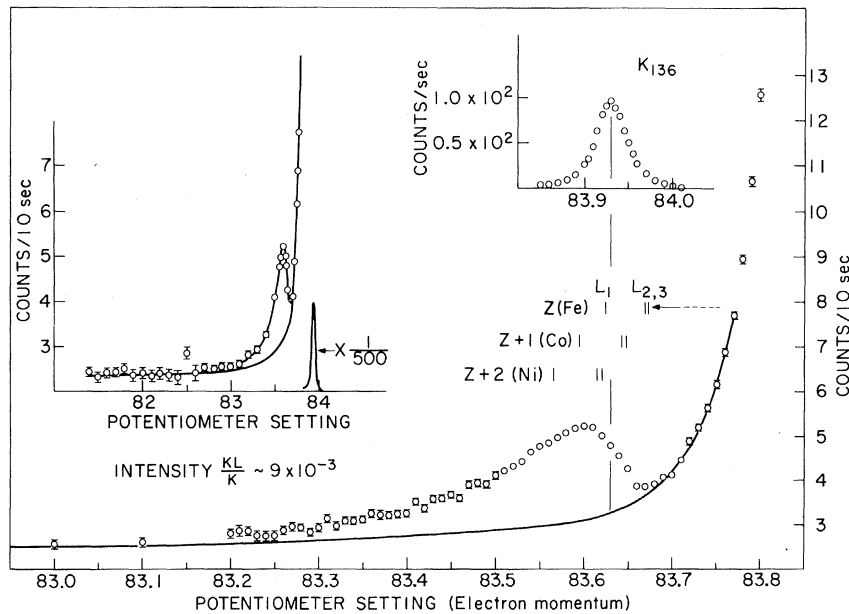


FIG. 4.  $KL$  shakeoff continuum from the 136-keV transition following the decay of  $\text{Co}^{57}$ . Same source as Fig. 2. See Fig. 2 caption for additional comments. Note the intensity ratio of  $KL/K$  is the same for this  $E2$  transition as for the predominantly  $M1$  122-keV transition. Note also that the displacement of the  $KL$  threshold (in energy) from the  $K_{136}$  peak is nearly the same as for the 122-keV transitions. This is evidence that these bumps are not focusing aberrations of the spectrometer (ghosts), which must appear at constant fractional momentum displacements, if at all. Nor are they likely to be fortuitously located conversion lines of unknown weak transitions in  $\text{Fe}^{57}$  or in impurities.

C. More Detailed Analysis of the *KL* Continuum

## 1. Binding Energies

One of the results of these measurements is the energy required to remove both a *K* and *L* electron simultaneously from the atom. Because of the less-than-perfect *K* screening of the *L* electrons, one might expect that the *KL* continuum would begin at an energy difference less than  $L_{B.E.}(Z+1)$  below the *K* line; the notation indicates the *L* binding energy in atom ( $Z+1$ ). Interestingly, our experiments indicate the *KL* continuum starts a little more than  $L_{B.E.}(Z+1)$  below the *K* line.

Because differences between *L* binding energies in atoms of neighboring *Z* for our cases are comparable with the instrumental linewidth, the instrumental resolution must be taken into account in deciding where the continuum begins. One method involves making semilogarithmic plots of the *KL* bumps and of the line shape of the *K* conversion lines, and graphically approximately matching the high-energy edges. In each of Figs. 3, 4, and 5 is indicated a *K*-line shape in the position which resulted from such a (semilogarithmic)

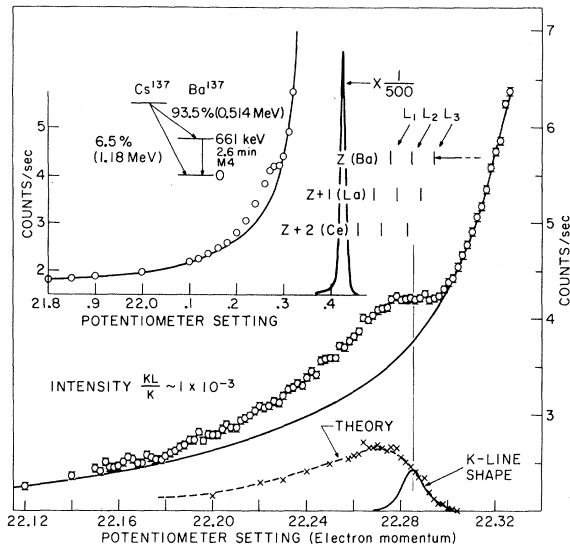


FIG. 5. *KL* shakeoff continuum from the 661-keV transition following the decay of  $Cs^{137}$ . The x marks are the result of subtracting the smooth continuation of the main *K*-line tail from the experimental points. The dashed curve marked theory is the result of folding the line shape with a calculated spectrum. The calculation assumed that each of the three components ( $KL_1$ ,  $KL_2$ , and  $KL_3$ ) has a shape given by Eq. (1), along with the Leviner  $2p$  result, Eq. (5). The ratio of the components used was 0.43:1:2, respectively, and the energy spacing of the components was the same as the *L*-subshell binding-energy spacing in Ba, but with the  $KL_3$  binding energy = 43.01 keV [i.e., threshold displacement from *K* line lies between  $L_3(La)$  and  $L_3(Ce)$ ]. The dashed curve is normalized to data points at the peak of the spectrum.

TABLE II. Experimental electron binding energies<sup>a</sup> in eV (neutral atom).

Atom \ Shell	<i>K</i>	<i>L</i> <sub>1</sub>	<i>L</i> <sub>2</sub>	<i>L</i> <sub>3</sub>
<sup>26</sup> Fe	7114	846	723	710
<sup>27</sup> Co	7709	926	794	779
<sup>28</sup> Ni	8333	1008	872	855

<sup>a</sup>Reference 19, Appendix 1, p. 224; see also J. A. Bearden and A. F. Burr, Rev. Mod. Phys. **39**, 125 (1967). Uncertainties are on the order of 1 eV.

graphical procedure. In each case, the peak of the line falls between  $L_{3B.E.}(Z+1)$  and  $L_{3B.E.}(Z+2)$  below the *K* line, thus indicating the energy at which the abrupt start of the continuum occurs. A more satisfactory analysis follows for the case of the *KL* continuum of the 122-keV transition in  $Fe^{57}$ .

Figure 6 shows the result from a source ~16 times stronger than that for Fig. 3. (We note that the *KL*/*K* intensity ratio is again  $\sim 9 \times 10^{-3}$ , independent of source strength and attendant variation in source thickness.) The *K* line is indicated in a position derived from the graphical procedure just described, but in Fig. 7 an "unfolding" is displayed which indicates the start of the continuum is closer to  $L_{3B.E.}(Z+1)$  than the graphical procedure indicates. The upper part of Fig. 7 displays the experimental points of Fig. 6 and a curve constructed by folding the "true spectrum" (labeled  $\sum KL$ ) in the lower part of Fig. 7 with the experimental line shape. This true spectrum is actually approached by a series of guesses. Each is folded (by computer integration) with the experimental line shape, and each generates a curve to be compared with the measured spectrum (with area normalization), the process being continued until a match within the statistical uncertainties of the measured points is obtained. Because the *KL* continuum must be made up of a contribution from each *L* subshell, the trial "true spectra" were chosen such that (1) the three separate subshell contributions would have the same shape, and (2) the relative energy positions (spacing) would be that of the *L*-subshell binding-energy differences at  $Z=26$ . The absolute position (abscissa in Fig. 7), the shape of the continua, and the relative intensity of  $KL_1$  to  $KL_2 + KL_3$  were varied until the result shown in Fig. 7 was obtained. The  $L_{2,3}$  spacing for this  $Z$  is too small to draw any conclusions concerning relative intensity from these data. The theoretical expectations based simply on number of electrons in each subshell is  $KL_3/KL_2$  (intensity) = 2 (which is shown in the curves of Fig. 7). On the other hand, the  $KL_1$  spacing is large enough to indicate with the as-

sumptions (1) and (2) just stated that the  $KL_1/(KL_2 + KL_3)$  intensity ratio is  $\sim 1/3$  that predicted<sup>10</sup> for the  $\beta^-$ -decay shakeoff of  $L$  electrons (see Table insert of Fig. 7). Further, it should be noted that acceptable fits can be found with even less  $KL_1$  bulge assumed in the trial spectrum, this being compensated by a more rounded shape at the peak of the distributions.

In spite of some ambiguity in the relative intensity of the subshell components, the unfolding procedure contributes an uncertainty of  $<5$  eV to the determination of the start of the  $KL_3$  continuum. Our result is that the  $KL_3$  continuum begins  $791_{-10}^{+20}$  eV below the  $K$  line. The uncertainty here is mostly due to the uncertainty in drawing in the back-scattering tail of the main  $K$  line. We have made no correction at the high-energy edge for excitation to unoccupied bound states. This correction is expected to be  $\sim 6$  eV and would, if discernible, increase our value of 791 eV. Table II gives the experimental binding energies for  $Z=26, 27, 28$ . The spacing between the  $KL_3$  continuum edge and the  $K$  line is seen, therefrom, to fall between the  $Z+1$  (Co) and  $Z+2$  (Ni) values for the  $L_3$  binding energy.

An equivalent way to state our results is that the total energy required to extract a  $K+L_3$  electron from the Fe atom<sup>11</sup> is  $7114 + 791 = 7905_{-10}^{+20}$  eV. This may be compared with a self-consistent-field calculation (SCF)<sup>12</sup> of this quantity which first finds the total energy of the electrons in the neu-

tral atom and then in the atom with a  $1s$  and a  $2p$  electron missing, the difference being the desired energy. This gives

$$\text{Fe(atom)} - \text{Fe}(1s)^{-1}(2p)^{-1} = 7887 \text{ eV},$$

$$\text{Experimental B.E. of } KL_3 = 7905 \text{ eV}.$$

However, the same procedure yields for the individual binding energies

$$\text{Fe(atom)} - \text{Fe}(1s)^{-1} = 7074 \text{ eV},$$

$$\text{Experimental B.E. of } K = 7114 \text{ eV},$$

$$\text{Fe(atom)} - \text{Fe}(2p)^{-1} = 729 \text{ eV},$$

Experimental mean B.E. of  $L_2$  and  $L_3 = 716$  eV.

Thus, the calculations underestimate the  $K$  binding energy by  $\sim 40$  eV and overestimate the  $L_{2,3}$  binding energy by  $\sim 13$  eV. If we make an empirical correction of  $40 - 13 = 27$  eV, the calculation yields  $7887 + 27 = 7914$  eV; not far off the experimental mark. As the techniques of SCF calculations are improved it will be interesting to see if these inner "double-vacancy" binding energies can be predicted accurately.

## 2. Spectrum Shape

As noted in the Introduction, the composite  $KL$  continuum can be regarded as the sum of two con-

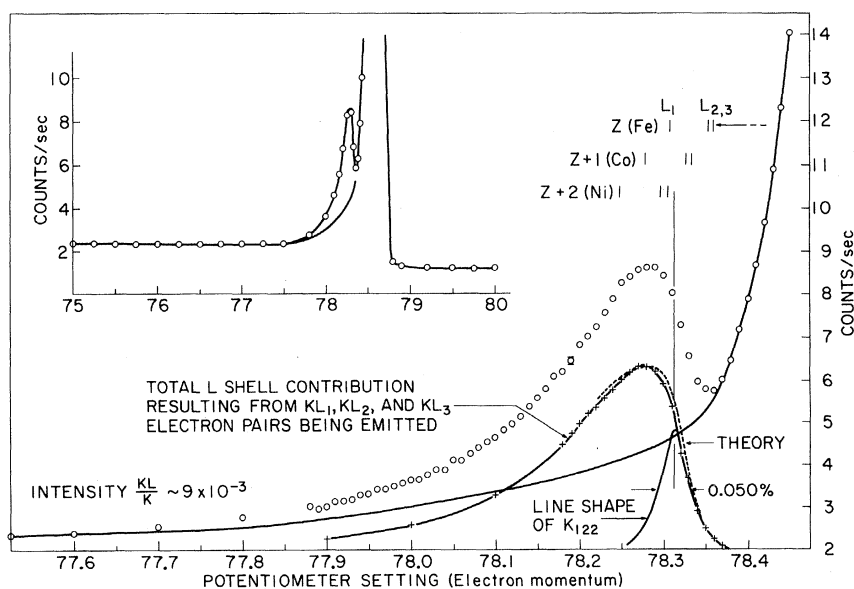


FIG. 6.  $KL$  continuum from the 122-keV transition following the decay of  $\text{Co}^{57}$ , from a source of  $\sim 80 \mu\text{Ci}$ . The + marks are the result of subtracting the smooth continuation of the tail of the  $K$  line from the experimental points. The curve labeled theory is the result of folding the  $K$ -line shape with a calculated spectrum made up of  $KL_1$ ,  $KL_2$ , and  $KL_3$  components (spaced as in Fe) in the ratio 0.43:1:2. The shape of each is taken from Eq. (1) with the Levinger  $2p$  result Eq. (5). The dashed curve is normalized to data at the peak of the spectrum.

tinua, one which dominates at low energy (we call this the shakeoff component), and its "mirror image" at the high-energy end of the continuum (the complementary partner component; see Fig. 1). In the lower part of Fig. 7, the shape of the resolution-corrected momentum spectrum of the complementary partner is seen in any one of the components, e.g.,  $KL_3$ . This spectrum, transformed to an energy spectrum<sup>13</sup> and reflected about the energy midway between zero and the maximum kinetic energy, is shown<sup>14</sup> in the upper part of Fig. 8. (The further transformation to a momentum spectrum is shown in the lower part of the figure.) Similar deductions of the experimental shakeoff spectrum have been carried out for the case of  $K$  photoionization by Krause, Carlson, and Dismukes.<sup>2</sup>

No one has carried out a calculation of the spectrum shape for the shakeoff electrons specifically associated with internal conversion, but from previous developments<sup>15-17, 5</sup> it can be inferred that the differential (in energy) spectrum will be proportional (i.e., electron-energy-independent factors are not included) to

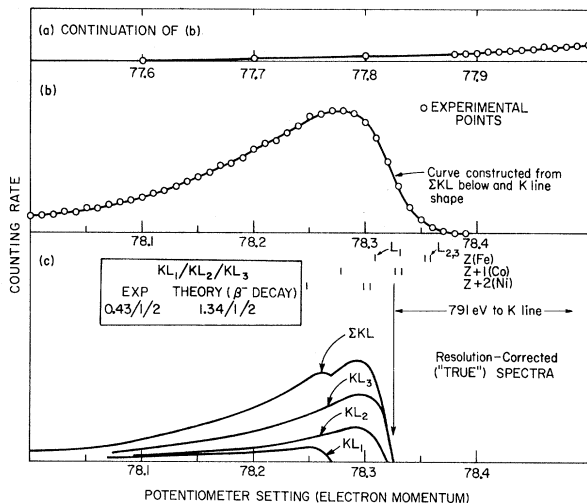


FIG. 7. (a)-(c) The resolution-corrected shapes of the  $KL$  continua of the 122-keV transition following the decay of  $Co^{57}$ . The lower curves (c) are arrived at through a series of trials, each trial being tested by folding it with the  $K$ -line shape (resolution function) and by comparing the result with the experimental points. The upper figures show this comparison; the experimental points are the same as the + marks of Fig. 6. The intensity ratio  $KL_3/KL_2$  is held fixed at 2/1, but the  $KL_1$  contribution is a variable. The table insert compares the result derived here with the expectations from the calculations of Carlson *et al.* (Ref. 10) for  $\beta^-$ -decay shakeoff. Another result derived here is the end point of the  $KL_3$  continuum, which in turn yields the  $KL_3$  double-vacancy binding energy =  $791^{+20}_{-10}$  eV + 7114 eV ( $K$  binding energy in Fe) =  $7905^{+20}_{-10}$  eV.

$$N(W, W_K)dWdW_K = \{F(Z_f, W)B(W)\} \\ \times pWp_KW_K\delta(A - W - W_K)dWdW_K. \quad (1)$$

Here the curly bracket is the square of an overlap integral between the initial bound state of the ejected electron and the final continuum state. The total energy ( $W$ ) and momentum ( $p$ ) of the ejected (shakeoff) electron have no subscript; corresponding quantities for the complementary companion have subscript  $K$ . The units used are such that  $m_0 = c = \hbar = 1$ , and  $W^2 = p^2 + 1$ . The Dirac  $\delta$  function  $\delta(A - W - W_K)$  ensures energy conservation. The constant  $A$  is given by

$$A = E_\gamma + 2 - B.E.,$$

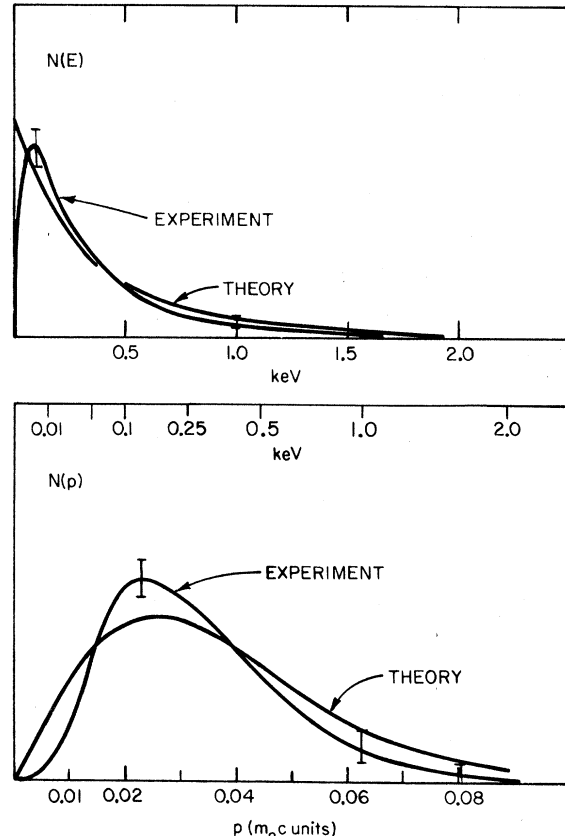


FIG. 8. Experimental shakeoff spectrum component of the  $KL_{122}$  continuum deduced from the  $KL_3$  resolution-corrected shape shown in the lower part of Fig. 7. The upper part of the figure gives the energy spectrum obtained from Fig. 7 (transformed to an energy spectrum) by reflection in the energy midway between zero and the end point of the continuum; the momentum spectrum shown below can then be derived from the upper curve. The curves labeled theory are Eqs. (2) and (6) using the Levinger  $2p$  result, Eq. (5); arbitrary normalization. Disparity between shape predictions of theory and experiment in the range  $p = (0-0.01)$  may be due to possible residual atomic excitation and ionization of  $Fe^{57}$  in the 136-keV state. [See Sec. II C(2).]

where  $E_\gamma$  is energy of the nuclear transition being internally converted, and B.E. is the energy required to remove simultaneously the  $K$  electron and the shakeoff electron from the atom. Both  $E_\gamma$  and B.E. are in  $m_0c^2$  units; the 2 is included for the rest mass of the two electrons. If expression (1) is integrated over  $W_K$ , the energy spectrum of the shakeoff electrons is obtained:

$$N(W)dW = \{F(Z_f, W)B(W)\} \\ \times pW[(A - W)^2 - 1]^{1/2}(A - W)dW, \quad (2)$$

where  $F(Z_f, W)$  is the "Fermi function" for the shakeoff electron in the final-state Coulomb field of some effective charge  $Z_f$  and is given approximately by the expression  $2\pi\alpha Z_f(W/p)[1 - e^{2\pi\alpha Z_f(W/p)}]^{-1}$ , or can be obtained from tables;  $\alpha \simeq \frac{1}{137}$ . The quantity  $B(W)$  depends on the initial state of the shakeoff electron and is given here for  $K(1s)$  electrons<sup>15-17</sup> and for  $L_1(2s)$  and  $L_{2,3}(2p)$  electrons<sup>17</sup> from nonrelativistic hydrogenic calculations.

For  $K(1s)$ ,

$$B(W) = \frac{\exp[-4\alpha Z_f(W/p)\tan^{-1}(y^{1/2})]}{(1+y)^4}. \quad (3)$$

with

$$y = \frac{(A - W_K)^2 - 1}{\alpha^2 Z^2} \approx \frac{(A - W_K)^2 - 1}{2 \times K_{B.E.}}$$

In Fig. 8 are shown the plots of expressions (2) and (6), using Eq. (5) for  $B(W)$ ;  $y = \frac{1}{2}p^2/(7.11/511)$ ;  $B.E. = 7.905/511$  and  $E_\gamma = 122/511$ . We chose the effective  $Z_f = 23$  for the  $2p$  electrons, as screened from the nuclear charge  $Z = 26$  in Fe (by the  $1s$ ,  $2s$ , and other  $2p$  electrons), by about three units.<sup>18</sup> The difference in theory and experiment in the region of 1 keV ( $p = 0.0625m_0c$ ) and higher may not be significant, since the choice of the underlying tail of the main line (see Fig. 6) has relatively wide range. However, the rise of the  $KL$  continuum as reflected in the region from 0-26 eV ( $p = 0-0.01$ ) of Fig. 8 is less steep in the experiment than in the theory (see also the Fig. 6 curve labeled theory). It is clear that different choices for the background curve will emphasize or minimize this discrepancy; however, the choice of background which would eliminate the discrepancy appears to us an unreasonable one. Factors which might cause such a discrepancy are: (1) failure to correct for excitation of  $L_{2,3}$  electrons to unoccupied bound states, (2) deficiency in the theory, and (3) some feature of the particular transition being studied.

With respect to this latter point, we note that

For  $L_1(2s)$ ,

$$B(W) = \frac{\exp[-4\alpha Z_f(W/p)\tan^{-1}(2y^{1/2})](3+4y)^2}{(1+4y)^6}. \quad (4)$$

For  $L_{2,3}(2p)$ ,

$$B(W) = \frac{\exp[-4\alpha Z_f(W/p)\tan^{-1}(2y^{1/2})](1+y)}{(1+4y)^6}, \quad (5)$$

where in expressions (3)-(5)

$$y = \frac{p^2}{\alpha^2 Z^2} \approx \frac{\text{ejected-electron kinetic energy}}{K_{B.E.} \text{ in nucleus with charge } Z}.$$

The momentum spectrum of the shakeoff electrons can be obtained from Eq. (2) [where  $dW = (p/W)dp$ ]:

$$N(p)dp = \{F(Z_f, W)B(W)\} \\ \times p^2[(A - W)^2 - 1]^{1/2}(A - W)dp. \quad (6)$$

The energy spectrum of complementary partner electrons can be obtained from Eq. (1) by integrating over  $W$  instead of  $W_K$ . We display here, as an example, the complementary spectrum for  $K$ -electron shakeoff

$$N(W_K)dW_K = F(Z_f, A - W_K) \exp\left\{-\frac{4\alpha Z_f(A - W_K)}{[(A - W_K)^2 - 1]^{1/2}} \tan^{-1}y^{1/2}\right\} \frac{[(A - W_K)^2 - 1]^{1/2}(A - W_K)}{(1+y)^4} p_K W_K dW_K, \quad (7)$$

the 136-keV level in  $Fe^{57}$ , from which the 122-keV transition arises (see Fig. 2), is populated mostly by  $K$ -electron capture. The vacancy thus created propagates outward in an Auger and x-ray cascade, resulting in ionized outer shells which may not have completely refilled by the time the 122-keV transition occurs. If the life time of the 136-keV level (8.9 nsec) is not long compared to the "recovery time" for the outer shells for the atom on a solid conducting substrate, the ensemble of decaying 136-keV states will have a range of binding energies for the inner shells reflecting the unsettled state of the valence shells. (The magnitude of the change in binding energies is of the order of 14 eV per charge removed from the valence shells.<sup>19</sup>) Thus, the experimental curve would be a composite of continua with different end points and would show a less sharp onset than for a case in which the ensemble of states has the same electron binding energies in the inner shells. We can bring no experimental evidence to bear on the question of the lifetime of valence-shell "holes" in Fe for our particular experimental conditions, so this explanation of the difference between theory and experiment is cer-

tainly not established.

In contrast, for the 661-keV transition in  $\text{Ba}^{137}$ , the question of a range of binding energies is completely suppressed because the state is very long lived (2.6-min half-life) compared to atomic recovery times, and because at this higher energy our instrumental resolution (linewidth) is very broad compared to the binding-energy variations caused by outer-shell vacancies. In Fig. 5, the curve marked theory is obtained by folding the instrumental resolution curve with the calculated spectrum. Within the statistical uncertainty, the theory describes well the shape of the *KL* continuum at the high-energy end. The "calculated spectrum" is a sum of three components in the ratio  $L_1:L_2:L_3=0.43:1:2$  chosen to be the same as that derived for the Fe case, but with spacing as in Ba. The  $KL_3$  binding energy from the fitting is  $43.01 \pm 0.03$  keV, compared with the sum,  $K_{\text{B.E.}}(\text{Ba}) + L_{3\text{B.E.}}(\text{La}) = 42.92$ , and a calculation<sup>12</sup> of the difference in total energies,  $\text{Ba}(\text{atom}) - \text{Ba}(1s)^{-1}(2p)^{-1} = 41.41$  keV.

#### D. *KK* Continua

Figure 2 shows an arrow pointing to the region on the combined backscattering tail of the main conversion lines where the *KK* bump is expected for the 122-keV transition in  $\text{Fe}^{57}$ , i.e., approximately the *K* binding energy in  $Z+1$  below the *K*

conversion line. The results of several weeks of counting in this region with an 80- $\mu\text{Ci}$  source are shown in Fig. 9 with coordinates expanded. On this scale, the interesting bulge in the backscattering tail, extending from 71 to 76 potentiometer units, barely discernible in Fig. 2, becomes obvious. Its origin is not understood. The feature which would be expected to indicate *KK* shakeoff is a step in the background continuum rising with the abruptness of the instrumental resolution function (see "*K*-line shape" in Fig. 9). The theoretical spectrum shape expectation, Eq. (7), folded with the line shape is shown at the bottom of Fig. 9. In the calculation we have used,  $E = \frac{122}{511}$  B.E. =  $\frac{14 \cdot 72}{511}$ ,  $Z_f = 26$ ,  $y = [(A - W_K^2) - 1] / (2 \times \frac{7 \cdot 11}{511})$ . The intensity is such that, when superimposed on the background continuum (dashed curve of Fig. 9), it represents an estimate for the intensity of the *KK* continuum consistent with our experimental points.

A serious experimental problem associated with this measurement was that the "background" continuum did not follow the  $\text{Co}^{57}$  half-life exactly; over a period of 30 days it showed less decay, i.e., 5.5% decay vs 7.5% expected for the 270-day half-life of  $\text{Co}^{57}$ . This suggested that the source was changing character, perhaps being covered by absorbed material from the residual vapor in the vacuum chamber of the spectrometer ( $5 \times 10^{-6}$  Torr). This would cause energy loss for some fraction of the conversion electrons, which would

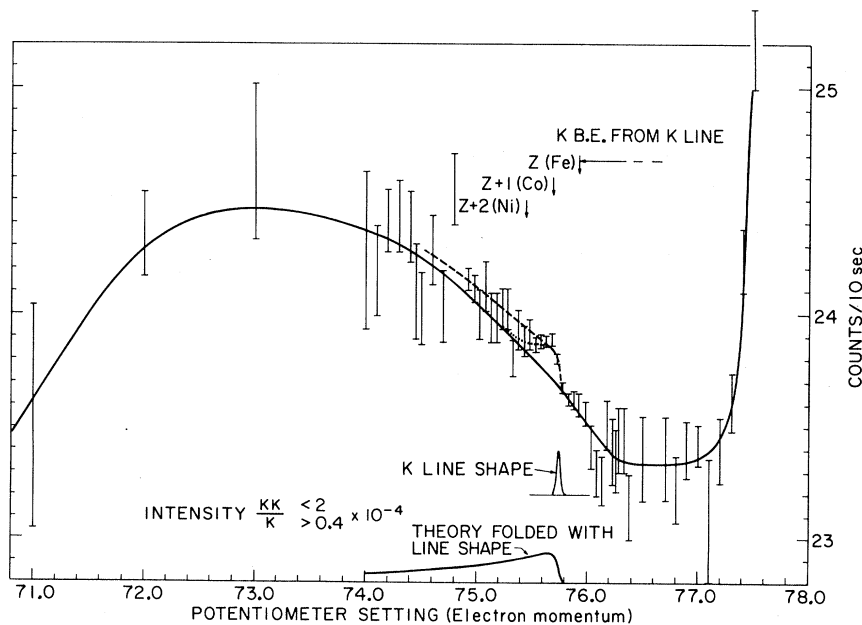


FIG. 9. Vertical expansion of counting rates in the neighborhood of the *KK* continuum end point for the 122-keV transition following the decay of  $\text{Co}^{57}$ . The broad bulge in the backscattering tail is barely visible in the Fig. 2 display for the same source. The dashed curve (lower curve labeled theory superimposed on the background bulge) is taken from Eq. (7), with intensity chosen to fit the rise at 75.75 potentiometer units; its area relative to the *K*-line area gives the upper limit for *KK* shakeoff indicated. The dotted curve we take as a lower limit.

TABLE III. Intensity of  $KK$  shakeoff relative to  $K$  conversion.

$Z^A$ (transition in keV)	Experiment $KK/K$	$K/\beta^-$ decay <sup>a</sup>	Theory $KK/K$ <sup>b</sup>
${}_{26}\text{Fe}^{57}$ (122)	$\begin{cases} <2 \\ >0.4 \end{cases} \times 10^{-4}$	$1.3 \times 10^{-3}$	$1.2 \times 10^{-4}$
${}_{56}\text{Ba}^{137}$ (661)	$<2 \times 10^{-4}$	$3.3 \times 10^{-4}$	$3.0 \times 10^{-5}$

<sup>a</sup>Reference 10. Calculation of shakeoff probabilities per  $\beta^-$  decay.

<sup>b</sup>Previous column multiplied by  $(0.3)^2$  to account for different effective change in charge ( $\beta^-$  decay vs  $K$  conversion) experienced by the  $K$  electron. See Ref. 10 and E. J. Seykora and A. W. Waltner, Am. J. Phys. **38**, 542 (1970).

then appear in the continuous tail forming the "background" for our measurements. This idea is supported by the fact that the 14-keV  $K$  line at 7 keV did, indeed, show an easily discernible decrease in peak height and increase in degraded tail during this period, as would be expected for this much lower-energy line if material were being absorbed onto the source. Although counting was done scanning back and forth over the region of interest, decay corrections were necessary to tie together all the data. These were made from effective-decay curves obtained from repeated counting in limited areas. In view of these difficulties, there is more uncertainty in the points than is indicated by the error bars in Fig. 9, which reflect only statistical counting errors.

From our data, the best estimate of the  $KK$  binding energy of Fe is  $14.72 \pm 0.15$  keV, compared with  $[K_{B.E.}(Z=26) + K_{B.E.}(Z+1)] = 14.82$  keV, or with calculated total energies<sup>12</sup>  $[\text{Fe}(\text{atom}) - \text{Fe}(1s)^{-2}]$

$= 14.50$  keV.

The dashed curve of Fig. 9 is taken as an upper limit for the  $KK$  shakeoff process. Its integrated area is listed in Table III. Curves with a much faster decrease in the  $KK$  continuum with energy could equally well be admitted by the experimental points. The dotted curve in Fig. 9 is such an example; its area is taken as the lower limit for the intensity in Table III.

For the higher- $Z$  case of the 661-keV transition in  $\text{Ba}^{137}$ , the  $KK$  bump is even more difficult to find. Figure 10 shows the result of several weeks of counting in the region of the  $K$  binding energy (in  $Z=56-58$ ) below the  $K$  line. Again, the theoretical shape prediction, folded with the  $K$ -line shape, is shown at the bottom of the figure with an intensity which yields  $KK/K = 1.2 \times 10^{-4}$ . We take about twice this value as an upper limit for  $K$  shakeoff accompanying  $K$  conversion in Ba. The theoretical estimate (see Table III, last column)

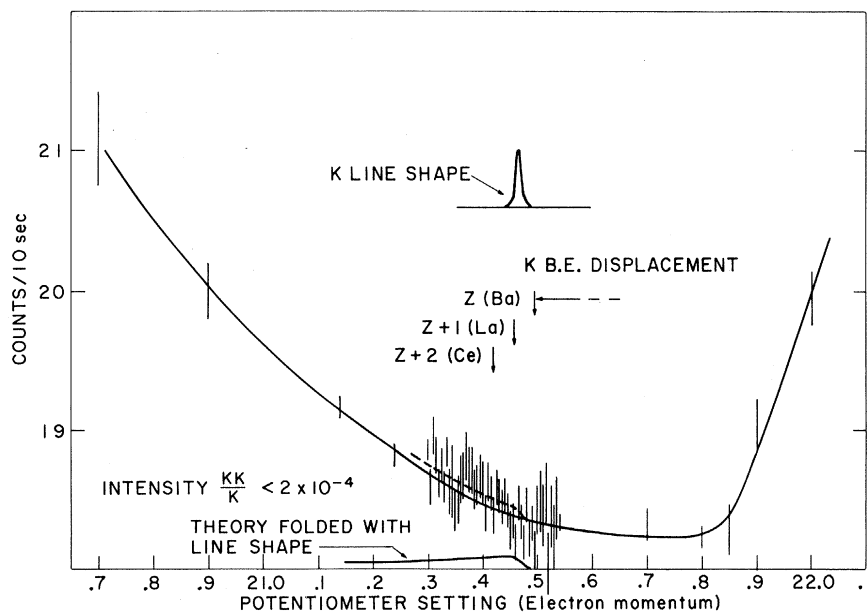


FIG. 10. Vertical expansion of the counting rate in the neighborhood of the  $KK$  continuum end point of the 661-keV transition following the decay of  $\text{Cs}^{137}$ . General background is the backscattering tail of the  $K$  line and the weak ground state  $\beta^-$  continuum. The curve indicated theory is from Eq. (7) with our choice of intensity; twice its area relative to the  $K$ -line area is taken as the upper limit indicated.

is an order of magnitude smaller.

In the Introduction, it was noted that the contribution of direct collisions might be significant in the  $KK$  continuum. For  $\beta^-$  decay the estimate<sup>4</sup> of the ratio of contributions was  $D.C./Sh \approx B.E./E$ . Applying this criterion for  $K$  conversion, one finds  $\frac{1}{14}$  and  $\frac{1}{18}$ , respectively, for the 122-keV transition in  $Fe^{57}$  and for the 661-keV transition in  $Ba^{137}$  using the  $K$  binding energies ( $B.E.$ ) and the  $K$ -conversion-line energies ( $E$ ). However, in Table III we have indicated that screening arguments predict that  $K$  ejection with  $K$  conversion is  $\sim \frac{1}{10}$  as probable as  $K$  ejection with  $\beta^-$  decay. If at the same time one argues that the D.C. contribution is the same for a  $K$  conversion electron and a  $\beta^-$  particle, then the D.C. contribution to the  $KK$  continuum would be the same order of magnitude as the shakeoff contribution. If a  $KK$  continuum is ever measured well enough, the spectrum shape can give the relative contributions. Feinberg's<sup>4</sup> Eqs. (15) and (16) give a spectrum shape which falls off less rapidly with energy than the shakeoff predictions.

#### E. 14-keV $K$ Conversion Line

We have looked for evidence of shakeoff accompanying  $K$  conversion of the 14-keV transition in  $Fe^{57}$ . In this case, there is not enough energy available for  $KK$ , and the  $KL$  continua fall near the  $KLM$  Auger lines, but  $M$ -shell shakeoff structure is expected in a position which would be favorable for observation. Figure 11 shows the  $K$  line of the 14-keV transition from a  $Co^{57}$  source deposited with the isotope-separator ions decelerated to  $<25$  eV onto the cleaved and etched surface

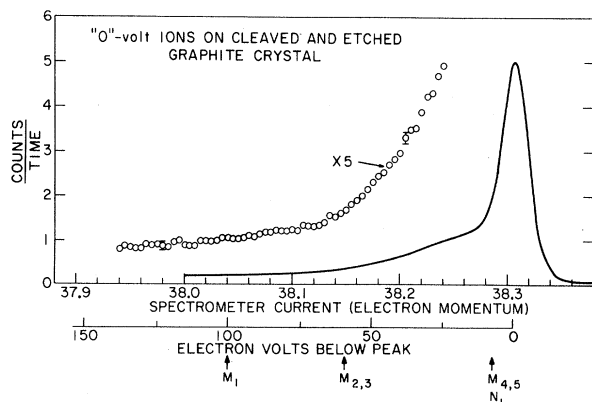


FIG. 11. The  $K$  conversion line of the 14.4-keV transition following the decay of  $Co^{57}$ . Arrows indicate regions near where  $KM$  shakeoff would be expected to begin. An intensity similar to that predicted for  $\beta^-$  decay (Ref. 10) would be visible on this scale (about 0.6 ordinate units for  $KM_{2,3}$  on the  $\times 5$  plot). It is not understood why the shakeoff is not seen here.

of a natural graphite crystal. These surfaces are believed to be smooth on the scale of a few atomic layers. The mean source thickness of this sample, on the basis of the time-integrated beam current at mass 57, is  $< \frac{1}{10}$  monolayer. In spite of such precautions, a low-energy tail with a large fraction of the total  $K$  electrons is evident. The tail extending to  $\sim 100$  eV below the  $K$  line is composed of electrons initially emitted into the acceptance solid angle of the spectrometer (rather than backscattered), since the tail intensity must be included with the main line to get agreement with the theoretical  $K$  conversion coefficient. The  $KM_1$  and  $KM_{2,3}$  shakeoff continua are expected to begin in the neighborhood of the arrows shown. The  $KM_{4,5} + KN_1$  bump would be too close to the main  $K$  line to be resolved. Why the  $KM_1$  and  $KM_{2,3}$  bumps are not evident is not understood. The expected intensities of 1 and 4%, respectively, relative to the  $K$  line are large enough to be seen easily if the expected shape of the shakeoff continuum occurred, even if it is folded with the experimental  $K$ -line shape. The available energy (7000 eV) is many times the binding energies of 50 and 100 eV, so that the criterion of Carlson, Moddeman, and Krause<sup>8</sup> (shakeoff processes are energy independent when the available kinetic energy is a few times the binding energy) is met. Moreover,  $KM$  continua in gaseous argon have been observed in photoelectric emission at  $\sim 1.3$  keV, with theoretically predicted intensity.

More cases with energy between 7 and 100 keV must be studied in order to decide whether some conceptual modification of the process is required, or whether solid-source effects are masking the shakeoff process at such low energy.

### III. CONCLUDING REMARKS

We have presented evidence that a  $KL$  shakeoff continuum accompanies  $K$  conversion lines at  $Z = 26$  (122 keV, mainly  $M_1$ ; and 136 keV,  $E_2$ ), and at  $Z = 56$  (661 keV,  $M_4$ ). The probability relative to the  $K$ -line intensity is in reasonable agreement with SCF overlap-integral predictions as modified with screening factors, and appears not to depend on the multipolarity of the transition. Although the shape of the continua of the complementary particle at the high-energy end is in general agreement with nonrelativistic calculations, detailed comparison has yet to be made at energies of the order of twice the binding energy away from the end point. What is required here is thinner backings to reduce the backscattering tail of the main line, whose subtraction leads to the large uncertainty in that region. With regard to the shape near the end point, a transition between 50 and 100 keV of half-

life  $>100$  nsec would be useful to resolve the question concerning neutralization of the atom in the isomeric state, which was raised in Sec. II C 2. Better measurements will also require some correction for excitation of the bound electron to unoccupied bound states.

Our preliminary look at  $KK$  continua indicates, again, much thinner backings are required to improve the signal-to-noise ratio. For higher- $Z$  cases, such as Ba considered here, the  $KK$  continuum may be very difficult to observe if the theoretical estimates of the intensity are correct. At our resolution (0.05%), the step in counting rate at the  $KK$  end point for Ba may be only  $10^{-6}$  of the peak rate.

The failure to find  $KM$  structure on the 14-keV  $K$  line might be an indicator of serious disagreement with shakeoff theory if it were not for the experience<sup>2,8</sup> with gaseous sources at an even lower energy relative to the binding energy. Instead, the anomaly probably points to some solid-source effect, as yet unexplained.

Shakeoff structure on other than  $K$  conversion lines is, of course, expected. For example, we can speculate that  $LL/L$  ratios will be small (small effective change in charge as in  $KK$ ), although  $L_1L_{2,3}/L_1$  may be larger than  $L_1L_1/L_1$ .

A final remark concerns the measurement of conversion-line areas for the purpose of determining absolute conversion coefficients or conversion-line ratios. If instrumental resolution is poor, the shakeoff structure may lie in the line area, but at better resolution the shakeoff structure represents a depletion of the line area. For example, for the 122-keV  $K$  line in Fe<sup>57</sup> examined here, if the  $KL$  bump is not included in the area, a 1% error is made.

#### ACKNOWLEDGMENTS

We are indebted to J. Lerner for many sources prepared on the Argonne electromagnetic isotope separator, and to M. Fred for arranging the SCF calculations of the double-vacancy binding energies.

\*Based on work performed under the auspices of the U. S. Atomic Energy Commission.

<sup>1</sup>There is considerable literature on this subject which we shall not quote exhaustively here. A review paper, which may be useful to those wishing to get an over-all view, can be found in the chapter by S. Wexler in *Actions Chimiques et Biologiques des Radiations*, edited by M. Haissinsky (Masson, Paris, France, 1965), Vol. 8, pp. 110-193.

<sup>2</sup>M. O. Krause, T. A. Carlson, and R. D. Dismukes, *Phys. Rev.* **170**, 37 (1968). At the high-energy end of the complementary spectrum, structure can be seen at high resolution which does not have a counterpart in the shakeoff (ionization) component, namely, lines ascribable to transitions of the second electron to unoccupied bound states. For the outer atomic shells such excitation can have significant intensity relative to the ionization probability. K. Siegbahn, C. Nordling, G. Johansson, J. Hedman, P. F. Hedén, K. Hamrin, U. Gelius, T. Bergmark, L. O. Werme, R. Manne, and Y. Baer [*Electron Spectroscopy for Chemical Analysis Applied to Free Molecules* (North-Holland Publishing Company, Amsterdam, The Netherlands, 1969), pp. 25, 30-36], working at higher resolution have shown clearly several lines assigned to transitions of  $L$  (valence) electrons to unoccupied bound states ("shakeup") accompanying  $K$  photoionization in neon.

<sup>3</sup>See for example J. Eichler, *Z. Physik* **160**, 333 (1960).

<sup>4</sup>E. L. Feinberg, *Yadern. Fiz.* **1**, 612 (1965) [transl.: *Soviet J. Nucl. Phys.* **1**, 438 (1965)].

<sup>5</sup>P. Stephan and B. Crasemann, *Phys. Rev.* **164**, 1509 (1967).

<sup>6</sup>P. Erman, B. Sigfridsson, T. A. Carlson, and K. Fransson, *Nucl. Phys.* **A112**, 117 (1968).

<sup>7</sup>H. J. Fischbeck, F. Wagner, F. T. Porter, and M. S.

Freedman, *Phys. Rev. C* **3**, 265 (1971).

<sup>8</sup>T. A. Carlson, W. E. Moddeman, and M. O. Krause, *Phys. Rev. A* **1**, 1406 (1970).

<sup>9</sup>M. S. Freedman, F. Wagner, Jr., F. T. Porter, J. Terandy, and P. P. Day, *Nucl. Instr. Methods* **8**, 255 (1960).

<sup>10</sup>T. A. Carlson, C. W. Nestor, Jr., T. C. Tucker, and F. B. Malik, *Phys. Rev.* **169**, 27 (1968).

<sup>11</sup>Our result, more correctly, is for the Fe atom in the oxidized state. We have shown in other experiments on the  $K$  line of the 14-keV transition that sources prepared in the manner described here yield  $K$  and  $L$  binding energies shifted by  $\sim 4$  eV from the metallic state, i.e., the electrons are more tightly bound in the oxidized state.

<sup>12</sup>Charlotte Froese Fischer program, revised by M. Wilson, a nonrelativistic numerical Hartree-Fock approach.

<sup>13</sup>A magnetic spectrometer output (the count spectrum) is a counting rate vs a number proportional to electron momentum  $p$ . Because the "window width"  $\Delta p = \text{constant} \times p$  for a magnetic spectrometer, the count spectrum divided by momentum at each point becomes the momentum spectrum  $N(p)$ . A transformation to the energy spectrum requires multiplying  $N(p)$  by  $W/p$ , where  $W$  is the total energy of the electron. Because of the fractional change in  $p$  and  $W/p$  is very small for a continuum extending a few hundred eV at 100 keV, the distinctions in shape between the count spectrum,  $N(p)$ , and  $N(W)$  are very small, but we make them formally. For a continuum extending a few hundred eV near zero energy, these distinctions in shape are very important. (See Fig. 8.)

<sup>14</sup>In this deduction of the shape of the shakeoff spectrum the contribution near the leading edge of the complementary spectrum which is associated with excitations of  $L$  electrons to unoccupied bound states is not subtracted. At our resolution this contribution is essentially a mono-

chromatic line at the upper limit of the continuum. From graphical manipulation we estimate our data cannot rule out an excitation contribution of ~5% of the total *KL* bump. Calculations using hydrogenic wave functions {G. A. Skorobogatov, *Teor. Eksperim. Khim.*, 2, 26 (1966) [transl.: *Theoret. Exptl. Chem.*, 2, 20 (1966)]} predict ~20% of the total *KL* area might be due to excitation to unoccupied bound states. Our spectrum shape is inconsistent with such a large fraction.

<sup>15</sup>E. L. Feinberg, *J. Phys. (USSR)*, 4, 423 (1941).

<sup>16</sup>H. Primakoff and F. T. Porter, *Phys. Rev.*, 89, 930 (1953).

<sup>17</sup>J. S. Levinger, *Phys. Rev.*, 90, 11 (1953).

<sup>18</sup>See for example A. H. Wapstra, G. J. Nijgh, and R. Van Lieshout, *Nuclear Spectroscopy Tables* (North-Holland Publishing Company, Amsterdam, The Netherlands, 1959), p.88: screening ~0.85 *Z* per *K* and 0.35 per other *L* electron.

<sup>19</sup>K. Siegbahn, C. Nordling, A. Fahlman, R. Nordberg, K. Hamrin, J. Hedman, G. Johansson, T. Bergmark, S.-E. Karlsson, I. Lindgren, and B. Lindberg, *Nova Acta Regiae Soc. Sci. Upsal.*, 20, 76 (1967).

## Low-Lying Levels of <sup>40</sup>Ar †

R. L. Place,\* K. H. Buerger, Jr., † T. Wakatsuki, § and B. D. Kern

*Department of Physics and Astronomy, University of Kentucky, Lexington, Kentucky 40506*

(Received 2 November 1970)

Seven excited levels of <sup>40</sup>Ar have been populated by the <sup>40</sup>Ar(*p, p'*) reaction and studied with  $\gamma$ - $\gamma$  and *p'*- $\gamma$  angular-correlation techniques. Spin-parity assignments are: 1461 keV, 2<sup>+</sup>; 2121 keV, 0<sup>+</sup>; 2524 keV, 2<sup>+</sup>; 2892 keV, (4)<sup>+</sup>; 3207 keV, 2<sup>+</sup> or 1<sup>±</sup>; 3507 keV, 2<sup>+</sup> or 1<sup>±</sup>; 3681 keV, 3<sup>-</sup>. Multipole amplitude mixing ratios are: 2524 → 1461-keV transition,  $\delta(E2/M1) = +0.24$ ; 3207 → 1461-keV transition, if 2<sup>+</sup> → 2<sup>+</sup>,  $\delta(E2/M1) = -0.20$ , and if 1<sup>±</sup> → 2<sup>+</sup>,  $\delta = 0$ .  $\gamma$ -ray branching ratios for the second to seventh excited levels have been measured. These results, together with lifetimes previously determined by others, are used to calculate *B*(*E2*) and *B*(*M1*) values which are compared with those of similar levels in <sup>42</sup>Ca.

### I. INTRODUCTION

In this study, <sup>40</sup>Ar spins and parities,  $\gamma$ -ray multipole amplitude mixing ratios, and  $\gamma$ -ray de-excitation branching ratios have been determined within the limits of available techniques. Levels of <sup>40</sup>Ar up to 3681 keV have been excited by the inelastic scattering of protons, and their decay modes have been observed with *p'*- $\gamma$  and  $\gamma$ - $\gamma$  coincidence techniques.

Previous measurements include a determination of the energies of many <sup>40</sup>Ar levels through use of the <sup>40</sup>Ar(*p, p'*) reaction by Benveniste, Booth, and Mitchell,<sup>1</sup> and a <sup>40</sup>Cl  $\beta$ -decay study<sup>2</sup> which complements the present work and which provides precise level energies as illustrated in Fig. 1. Earlier work has been summarized by Endt and van der Leun<sup>3</sup> and in Ref. 2. Recently, measurements have been made of branching ratios<sup>4, 5</sup> and of the lifetimes of the first three excited levels.<sup>5, 6</sup> Differential cross sections for the <sup>40</sup>Ar( $\alpha, \alpha'$ ) reaction have been measured and interpreted.<sup>7</sup> Proton-hole states have been investigated through the <sup>41</sup>K(*d, <sup>3</sup>He*)<sup>40</sup>Ar reaction.<sup>8</sup> Spin assignments have been based on the analysis<sup>9</sup> of (*p, p'*) angular distributions which were obtained using 24.85-MeV protons. Not all of the previous

reports on the properties of <sup>40</sup>Ar levels are in agreement; some of them will be discussed in Secs. IV and V in connection with the present results. Theoretical calculations of the structure of <sup>40</sup>Ar have been few in number.<sup>6, 10-14</sup> Since <sup>40</sup>Ar has two *d*<sub>3/2</sub> proton holes and two *f*<sub>7/2</sub> neutron particles, the large-scope shell-model calculations have omitted this "transition" nucleus.

### II. EXPERIMENTAL PROCEDURES

Protons from the University of Kentucky 6-MV Van de Graaff accelerator, having energies in the range from 4.7 to 5.8 MeV, were used to bombard a target of gaseous argon at typical pressures of 12 to 20 cm of Hg. After being energy-analyzed by a 90° bending magnet the proton beam was converged by a magnetic quadrupole doublet to a target position which was 14 m from the bending magnet. The gaseous argon was contained within a small cell which was inside of a 12.70-cm-diam aluminum scattering chamber. The cell itself was an aluminum cylinder with height of 1.98 cm and outside diameter of 1.4 cm, closed at the top end and attached to the gas supply system at the lower end. There was a 0.48-cm-wide opening cut in the cell wall, circumferentially